MASSIVE SEPARATION OF TURBULENT COUETTE FLOW IN A ONE-SIDED EXPANSION CHANNEL

George K. El Khoury and Bjørnar Pettersen
Department of Marine Technology,
The Norwegian University of Science and Technology
NO-7491 Trondheim, Norway
george@ntnu.no

Mustafa Barri and Helge I. Andersson
Department of Energy and Process Engineering,
The Norwegian University of Science and Technology
NO-7491 Trondheim, Norway
barri@ntnu.no

ABSTRACT

Direct numerical simulation has been performed to study wall-driven flow over a backward-facing step at Reynolds number $Re = 5200$ based on the step height h and the upper wall velocity U_w. The flow configuration consisted of a step with height equal to that of the upstream channel yielding an expansion ratio $2:1$. The instantaneous enstrophy contours revealed the formation of Kelvin-Helmholtz instabilities downstream of the step. A fully redeveloped Couette flow cannot be reached in the downstream part of the channel due to mass conservation. The local wall pressure coefficient gave evidence of an adverse pressure gradient in the recovery region where a Couette-Poiseuille flow type prevailed. The budgets for the Reynolds shear-stress and turbulent kinetic energy have been computed. In the mixing layer, the peak production of turbulent kinetic energy was 2.5 times larger than that of viscous dissipation.

INTRODUCTION

Turbulent flow over a backward-facing step (BFS) is a simplified case of the general family of separated flows with widespread industrial applications. Although its geometry is simple, the flow physics is still complex. Typical prototypes of BFS flows are the boundary layer, the plane channel and the Couette flow cases, see e.g. (Eaton and Johnston, 1981). A common feature of these flows is the existence of a shear layer emanating from the step corner and reattaching further downstream leading to the formation of a recirculation bubble. The presence of the internal shear layer and the massive recirculation zone gives rise to complex flow dynamics which for instance affect the turbulence production and Reynolds stress anisotropy.

The most studied BFS flow is the pressure-driven flow in a plane channel with a sudden one-sided expansion. Due to the principle of mass conservation, the Reynolds number remains the same downstream of the step as in the upstream part of the channel. In a BFS Couette flow, on the other hand, the Reynolds number becomes higher downstream of the step. It is well known that the shear-driven turbulent Couette flows (Bech et al., 1995) exhibit a number of characteristic features which make them distinguishingly different from the pressure driven Poiseuille flow, notably the monotonically increasing mean velocity profile. The only investigation of BFS Couette flow we are aware of is the re-
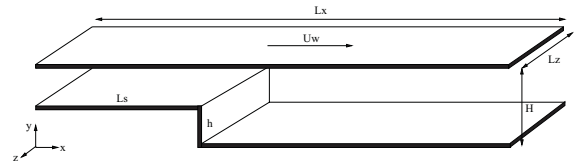

Figure 1: Flow configuration.

cent experimental study by Morinishi (2007). He considered a configuration with the step height h equal to half of the upstream channel height, i.e. with an expansion ratio 3:2. The upstream Reynolds number was about 24000.

In the present study we perform direct numerical simulation (DNS) of turbulent Couette flow over a BFS. This will enable us to gather accurate mean flow and turbulence statistics throughout the flow domain, as well as to explore in detail the instantaneous vortex topology in the mixing layer and the recirculation bubble as well as in the reattachment zone. We intentionally considered a BFS configuration where the flow upstream of the step is the same as studied by Bech et al. (1995).

METHOD

Flow configuration and governing equations

Figure 1 shows a schematic view of the Couette backward-facing step flow which is composed of a step of height h and an upper wall moving with velocity U_w. Of particular relevance in backward-facing step flows is the expansion ratio ER. This dimensionless parameter is defined as the ratio between the downstream and upstream channel heights, i.e. $ER = H/(H - h)$. In the present study we consider a flow configuration where the step height is equal to that of the upstream channel, i.e. $H = 2h$. This gives an expansion ratio of $2:1$.

The governing equations are the time-dependent, incompressible Navier-Stokes equations for a viscous fluid expressed in non-dimensional form:

$$\nabla \cdot \mathbf{u} = 0 \tag{1}$$

$$\frac{\partial \mathbf{u}}{\partial t} + (\mathbf{u} \cdot \nabla)\mathbf{u} = -\nabla p + \frac{1}{Re}\nabla^2 \mathbf{u} \tag{2}$$

Table 1: Computational parameters.

Re	$N_x \times N_y \times N_z$	Δx^+	Δy^+	Δz^+
5200	$672 \times 384 \times 192$	4.8-14.8	0.083-4.2	8.2

Here, the variables have been non-dimensionalized by h and U_w and the Reynolds number based on the step height and upper wall velocity, $Re = U_w h/\nu$, is 5200.

Numerical approach

The computational domain has a length of $L_x = 39h$ in the streamwise $x-$direction including an inlet section $L_s = 15h$, $H = 2h$ in the wall-normal $y-$direction, and $L_z = 9.43h$ in the spanwise $z-$direction.

No-slip boundary conditions are imposed at all the wall surfaces. In the spanwise direction, the flow is assumed to be statistically homogeneous and periodic boundary conditions are used. A realistic fully turbulent flow is generated at the input by recycling finite-length time series of the instantaneous velocity planes. This technique was first used by Barri et al. (2008) in a numerical simulation of plane channel flow. At the exit, we solve the convective equation $\partial\mathbf{u}/\partial\mathbf{t} + U_c\partial\mathbf{u}/\partial x = 0$ to ensure a proper outflow condition. This type of boundary condition was used in previous numerical simulations by (Lowery and Reynolds, 1986) for mixing layer and (Le et al., 1997) for turbulent flow over a backward-facing step and is considered suitable for vortical structures moving out of the domain.

A non-uniform mesh is employed in the streamwise and wall-normal directions in order to adequately resolve the turbulence scales in the separation region and the vicinity of the walls whereas a uniform mesh is used in the spanwise direction. The detailed computational parameters are shown in table 1 where the grid spacing is measured in wall units using the viscous length scale $l_i = \nu/u_{\tau i}$ based on the wall-friction velocity at the input $u_{\tau i} = 0.032U_w$.

The DNS code used to numerically solve the governing equations 1 and 2 is MGLET (see Manhart, 2004). MGLET is a finite-volume code in which the Navier-Stokes equations are discretised on a staggered Cartesian mesh with non-equidistant grid-spacing. The discretisation is second-order accurate in space. A second-order explicit Adams-Bashforth scheme is used for the time integration. The Poisson equation for the pressure is solved using a multi-grid algorithm.

The simulations were started from an arbitrary flow field and thereafter let to evolve to a statistically steady state. The time step used was $\Delta t = 0.001h/U_w$. Statistics were gathered for a period of $396h/U_w$ after the flow field first had evolved into a statistically steady state.

RESULTS AND DISCUSSIONS

Transverse vortices are a commonly observed feature in turbulent shear flows. Nychas et al. (1973) showed that the underlying mechanism in the formation of such vortical structures is a Kelvin-Helmholtz instability and is associated with wall region ejection. An outward displacement of low-speed fluid from the near wall region and an inward motion of high-speed fluid result in an interface where two streams of fluid move almost parallel to each other with different velocities. This interface between the high- and low-speed fluid region, being unstable, can lead to such a vortex formation. In backward-facing step flows, the forma-
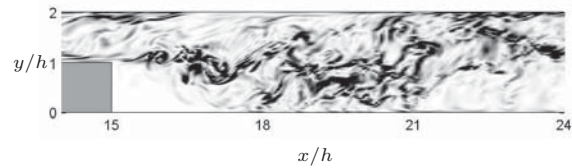

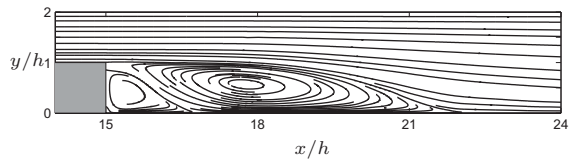Figure 2: Instantaneous enstrophy contours.
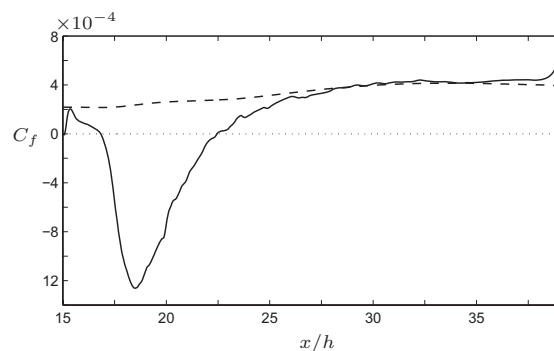

Figure 3: Streamlines of the mean flow.

Figure 4: Skin friction coefficient variation downstream the step: ———, Lower wall; $----$, Upper wall (divided by a factor of 10).
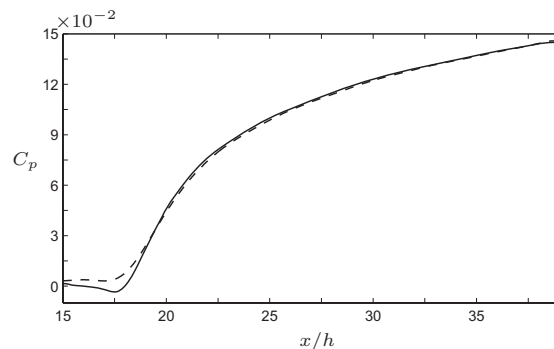

Figure 5: Pressure coefficient variation downstream the step: ———, Lower wall; $----$, Upper wall.

tion of Kelvin-Helmholtz (K-H) vortices takes place behind the step and were observed by Neto et al. (1973).

In order to see whether or not K-H vortices are embedded in the present flow field, the instantaneous contours of enstrophy are plotted in an $(x, y)-$plane in figure 2. There is an apparent roll-up of the shear layer behind the step edge where the unsteady K-H vortices are generated and break up into numerous small high-intensity vortices as they are transported downstream. This flow pattern phenomenon is caused by the Kelvin-Helmholtz instability where the oscillations induced by the latter are due to the interaction between the shear layer and the re-circulating region near the step.
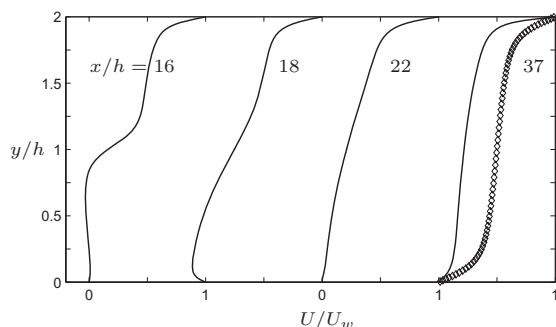
Figure 6: Mean streamwise velocity profiles. The symbols denote DNS data from Bech et al. (1995).

Figure 7: Turbulent intensities scaled with the upper wall velocity U_w. ———, streamwise direction; $\cdots\cdots$, wall-normal direction; $----$, spanwise direction.

Figure 8: Reynolds shear stress $-\overline{uv}/U_w^2$.

Mean statistics

From pressure-driven BFS flows it is known that the unsteady behaviour of the shear layer causes the reattachment line to fluctuate around a mean value X_R, see e.g. (Friedrich and Arnal, 1991). The streamline pattern of the mean flow in figure 3 shows a large primary separation bubble which extends about $7.5h$ downstream of the step. A secondary bubble of length $1.78h$ can be observed adjacent to the corner. The skin friction coefficient, defined as $C_f = \tau_w/\frac{1}{2}\rho U_w^2$, is shown in figure 4 and confirms that a secondary separation bubble with anti-clockwise flow ($C_f > 0$) is embedded within the primary separation bubble with clockwise motion ($C_f < 0$). This flow pattern is consistent with the findings of Morinishi (2007) who reported that reattachment occurred at $X_R = 6.63h \pm 1.4h$ and the secondary bubble was at $1.88h \pm 0.4h$. Downstream of $x/h = 30$, C_f is almost constant along both walls with the wall-friction along the moving surface being about 10 times higher than at the lower surface. This suggests a substantial asymmetry of the mean velocity field.

The local wall pressure coefficient is defined as $C_p = (P - P_o)/\frac{1}{2}\rho U_w^2$ where P_o is a reference pressure taken at $x/h = 5$. In figure 5, C_p exhibits a local minimum close to the position of maximum backflow (i.e. beneath the core of the primary separation bubble). Downstream of $x/h = 30$, an almost linear variation of C_p is observed. This implies that the streamwise mean pressure gradient has become independent of x and the flow field can be considered as being nearly fully developed in the downstream part of the computational domain. This is consistent with the constancy of C_f observed in figure 4.

Figure 6 presents the mean streamwise velocity profiles at four representative locations: inside the secondary bubble, through the primary recirculation, downstream of the reattachment and in the recovery region. Although the characteristic S-shape of the mean velocity profile $U(x, y)$ has been retained at $x/h = 37$, the profile is yet far from being anti-symmetric. Midway between the walls U is still roughly half of $1/2U_w$ which should be reached in the case a fully re-developed Couette flow. However, irrespective of the length of the domain that can be used in the downstream part of the channel, an anti-symmetric profile corresponding to a fully re-developed Couette flow will not be reached. This is due to the principle of mass conservation. It follows that since the height of the domain after the step is twice that of the inlet section and the mean velocity profile of Couette flow is monotonically increasing to a constant value of U_w, the flow cannot adjust itself to an anti-symmetric S-profile shape and at the same time maintain a conserved flow rate. In the recircul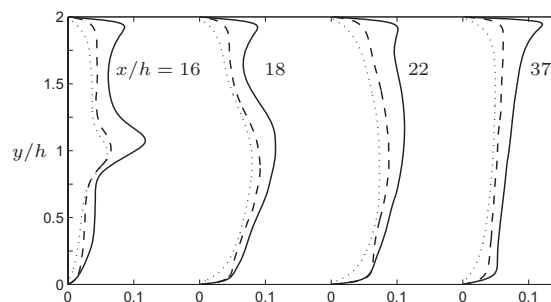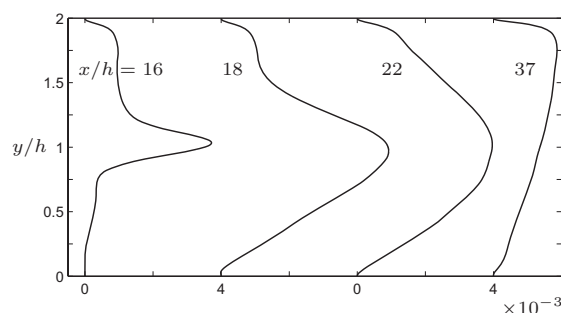ation region the strongest backflow is observed beneath the core of the primary bubble, whereas the secondary separation region shows a weak mean-streamwise motion.

The turbulence intensities and the Reynolds shear stress are shown in figures 7 and 8 at different streamwise locations downstream of the step. Although the $r.m.s$ values and $-\overline{uv}$ fall approximately to zero in the secondary recirculation region indicating a laminar-like flow, they exhibit a high turbulence level immediately downstream of the step at $y/h \approx 1$. This localized high-turbulence zone, mainly for u_{rms}, is obviously caused by the locally high mean-shear-rate in the mixing layer emanating from the step edge. As the flow progresses downstream, the streamwise turbulence intensity peaks are broaden and attenuated while the turbulence levels of the spanwise and wall-normall components increase. Downstream the reattachment and in the recovery region, the discrepancy in u_{rms} between the two walls persists where a substantially higher longitudinal turbulence intensity is observed near the moving wall that is almost twice that seen near the stationary wall.

The turbulence exhibits everywhere the usual shear-flow anisotropy with the streamwise intensity being the most significant. The profiles of $-\overline{uv}$ show that the Reynolds shear stress is positive almost throughout the whole domain.

The two-dimensional mean flow has developed to an essentially uni-directional flow in the downstream part of the computational domain, i.e. beyond $x/h \approx 30$ or 15 step heights h downstream of the sudden expansion. It is noteworthy that the upstream pure Couette flow redeveloped into a mixed Couette-Poiseuille flow in contrast to the classical pressure-driven backward-facing step flow where an upstream Poiseuille flow inevitably redevelops to another pure Poiseuille flow far downstream of the step. In the present case, however, an adverse pressure gradient is established with the view to assure global mass conservation. The resulting mixed Couette-Poiseuille flow exhibits major asym-
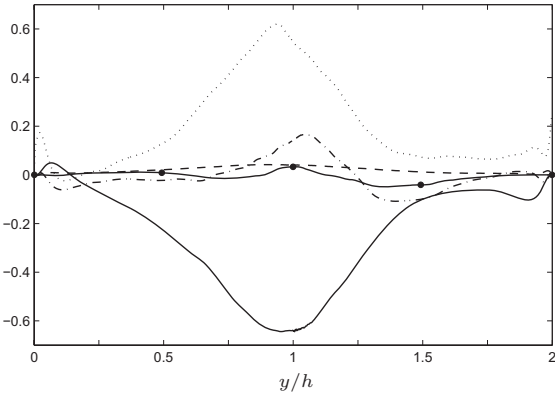
Figure 9: $\overline{uv}$ budget normalized by $u_{\tau i}^4/\nu$ at $x/h = 18$. ———, P_{ij}; — — —, $-\epsilon_{ij}$; ·······, Π_{ij}; — · —, T_{ij}; —●—, $U_k \partial(\overline{u_i u_j})/\partial x_k$.

metries in the turbulence field with a substantially reduced turbulence level along the stationary wall. The resulting flow field closely resembles the Couette-Poiseuille flow simulations reported by Kuroda et al. (1995).

Kinetic energy and shear stress budget

In this section, the budgets for the Reynolds shear stress and the turbulent kinetic energy are presented at a streamwise position passing through the center of the primary separation zone (i.e. $x/h = 18$). The transport equations for the Reynolds stress tensor are

$$\frac{D}{Dt}(\overline{u_i u_j}) = P_{ij} - \epsilon_{ij} + \Pi_{ij} + G_{ij} + D_{ij} + T_{ij} \qquad (3)$$

where

Production term:

$$P_{ij} = -\overline{u_i u_k}\frac{\partial U_j}{\partial x_k} - \overline{u_j u_k}\frac{\partial U_i}{\partial x_k} \qquad (4)$$

Dissipation term:

$$\epsilon_{ij} = 2\nu\overline{\frac{\partial u_i}{\partial x_k}\frac{\partial u_j}{\partial x_k}} \qquad (5)$$

Pressure-strain term:

$$\Pi_{ij} = \frac{1}{\rho}\left(\overline{p\frac{\partial u_i}{\partial x_j}} + \overline{p\frac{\partial u_j}{\partial x_i}}\right) \qquad (6)$$

Pressure diffusion term:

$$G_{ij} = -\frac{1}{\rho}\left(\frac{\partial}{\partial x_i}\overline{pu_j} + \frac{\partial}{\partial x_j}\overline{pu_i}\right) \qquad (7)$$

Molecular diffusion term:

$$D_{ij} = \nu\frac{\partial^2}{\partial x_k^2}\overline{u_i u_j} \qquad (8)$$

Turbulent diffusion term:

$$T_{ij} = -\frac{\partial}{\partial x_k}\overline{u_i u_j u_k} \qquad (9)$$

The budget for the turbulent kinetic energy $\overline{q^2}/2 = \overline{u_i u_i}/2$ is one half the sum of the budget of the diagonal components of the Reynolds stress tensor.
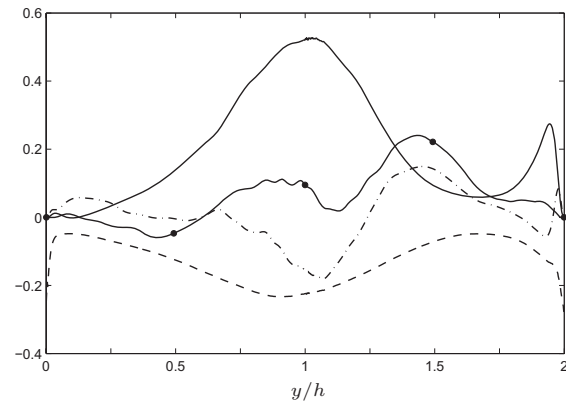

Figure 10: Turbulent kinetic energy budget normalized by $u_{\tau i}^4/\nu$ at $x/h = 18$. ———, P_K; — — —, $-\epsilon_K$; — · —, T_K; —●—, $U_k \partial(q^2/2)/\partial x_k$.

In figure 9, the equation for $\overline{uv}$ is largely dominated by production and pressure-strain where a large peak of negative production is observed at $y/h \approx 1$ that is balanced by the pressure-strain term. Apart from a small region near the lower wall, P_{12} is negative everywhere. The expression for this production term is

$$P_{12} = -\overline{uv}\frac{\partial U}{\partial x} - \overline{vv}\frac{\partial U}{\partial y} - \overline{uu}\frac{\partial V}{\partial x} - \overline{uv}\frac{\partial V}{\partial y} \qquad (10)$$

Since the mean flow is statistically two-dimensional, the first and fourth terms of equation 10 add up to zero due to mass conservation. This implies that the change of sign of P_{12} depends solely on the gradients of the mean streamwise and wall-normal velocities. $\partial U/\partial y$ being dominant over all the other mean gradient terms in this region, then equation 10 reduces to

$$P_{12} \approx -\overline{vv}\frac{\partial U}{\partial y} \qquad (11)$$

The above equation shows that the production of the Reynolds shear stress at $x/h = 18$ is dominated by $\partial U/\partial y$. Between $y/h = 0$ and $y/h \approx 0.2$, there is positive production of $\overline{uv}$ due to $\partial U/\partial y$ being negative. This indicates a negative Reynolds shear stress in that region. The change of sign of P_{12} occurs when $\partial U/\partial y$ is equal to zero, and the peak production is attained where $\partial U/\partial y$ exhibits a local minimum in the shear layer.

The turbulent diffusion contributes to the increase of Reynolds stresses in the central region whereas the viscous dissipation is negligible almost everywhere in this case. The nearly negligible viscous dissipation is consistent with the observation made by (Bech and Andersson, 1996) in a fully developed Couette flow. This is because ϵ_{12} consists of relatively weakly correlated velocity gradients.

The budget for the turbulent kinetic energy is shown in figure 10 at $x/h = 18$. In the shear layer, production and dissipation are the most dominant terms whereas turbulent diffusion transports energy into the upper half part of the channel only. The contribution to P_K comes mainly from P_{11} (see figure 11) and its peak at $y/h \approx 1$ is almost 2.5 times larger than that of ϵ_K. This infers that dissipation is not in balance with production.

In the regions close to the wall, turbulence is substantially damped along the lower one due to recirculation where production and turbulent diffusion are almost negligible in contrast to viscous dissipation which is the most significant
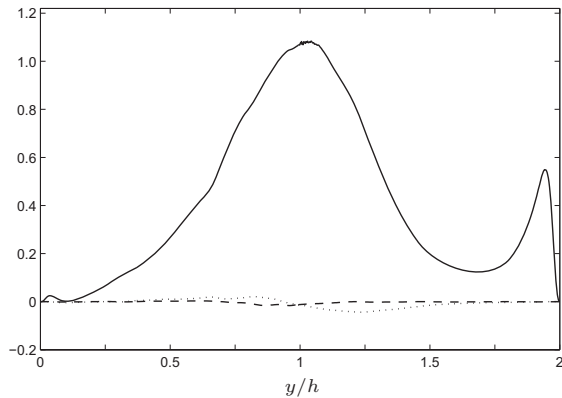
Figure 11: Turbulent production terms normalized by $u_{\tau i}^4/\nu$ at $x/h = 18$. ———, P_{11}; $\cdots\cdots$, P_{22}; $---$, P_{33}.
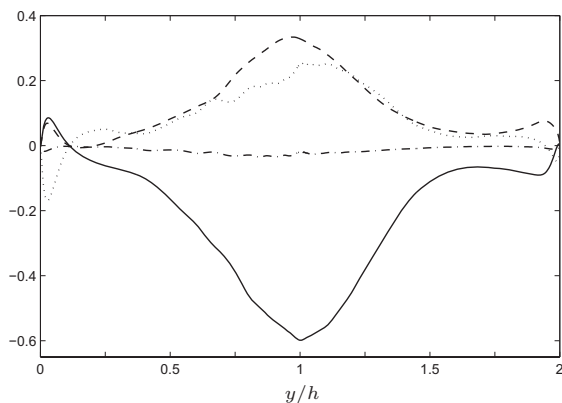

Figure 12: Pressure-strain terms normalized by $u_{\tau i}^4/\nu$ at $x/h = 18$. ———, Π_{11}; $\cdots\cdots$, Π_{22}; $---$, Π_{33}; $-\cdot-$, Π_{ii}.

(among the plotted terms). Along the upper wall, on the other hand, there is turbulent diffusion from the maximum source region towards and away from the walls and ϵ_K grows rapidly with y/h attaining a maximum value at the solid surface.

Since there is nearly no production of $\overline{v^2}$ and $\overline{w^2}$ as can be inferred from figure 11, their only source of energy is from Π_{ij} which serves to redistribute energy between the normal stresses. This is shown in figure 12 where the pressure-strain terms appearing in the $\overline{u^2}$, $\overline{v^2}$ and $\overline{w^2}$ equations are plotted together at $x/h = 18$. Across the channel, $\overline{ww}$ acts as a receiving component taking energy mainly from $\overline{uu}$. The profiles of Π_{11} and Π_{22} indicate a qualitative difference in the energy exchange pattern between the two walls. While there is a large energy transfer from the $\overline{vv}$ component to the $\overline{uu}$ and $\overline{ww}$ between $y/h = 0$ and $y/h \approx 0.2$, $\overline{uu}$ contributes to $\overline{vv}$ in delivering energy to $\overline{ww}$ in the region near to the upper wall. Away from the walls, the major effect of the pressure-strain is to distribute energy from $\overline{uu}$ component to the other two components. The sum of the three components (i.e. Π_{ii}) is almost zero and this supports the adequacy of the sampling procedure.

CONCLUSIONS

A direct numerical simulation of turbulent Couette flow over a backward-facing step has been performed at a low Reynolds number. The mean reattachment length of the shear layer was found to be $7.5h$. In the recirculation zone a large negative skin friction coefficient was observed beneath the core of the primary separation bubble.

The budgets for the Reynolds shear-stress and turbulent kinetic energy were computed. The production of turbulent kinetic energy was mostly into the streamwise normal stress where the loss of kinetic energy from the mean flow resulted in a gain in $\overline{uu}$ that was subsequently redistributed to the $\overline{vv}$ and $\overline{ww}$ through the pressure-strain correlation.

In the recovery region, the mean velocity profile did not retain the characteristic shape of pure Couette flow due to mass conservation, while Reynolds stresses showed that turbulence was substantially damped along the lower wall and correspondingly enhanced near the moving surface due to the increase in Reynolds number.

REFERENCES

Barri, M., El Khoury, G. K., Andersson, H. I., and Pettersen, B., 2008, "Inflow conditions for inhomogeneous turbulent flows", *Int. J. Numer. Meth. Fluids*, DOI: 10.1002/fld.1884.

Bech, K. H., Tillmark, N., Alfredsson, H., and Andersson, H. I., 1995, "Investigation of turbulent plane Couette flow at low Reynolds numbers", *J. Fluid Mech.*, Vol. 286, pp. 291-325.

Bech, K. H., and Andersson, H. I., 1996, "Structure of Reynolds shear stress in the central region of plane Couette flow", *Fluid Dynamics Research.*, Vol. 18, pp. 65-79.

Eaton, J. K., and Johnston, J. P., 1981, "A review of research on subsonic turbulent flow reattachment", *AIAA Journal*, Vol. 19, pp. 1093-1100.

Friedrich, R., and Arnal, M., 1991, "Analysing turbulent backward-facing step flow with the lowpass-filtered Navier-Stokes equations", *J. Wind Engng Indust. Aerodyn*, Vol. 35, pp. 101-128.

Kuroda, A., Kasagi, N., and Hirata, M., 1995, "Direct numerical simulation of turbulent plane Couette-Poiseuille flows: effect of mean shear rate on the near-Wall turbulence structures", *Turbulent Shear Flows 9, Springer-Verlag, Berlin*, pp. 240-257.

Le, H., Moin, P., and Kim, J., 1997, "Direct numerical simulation of turbulent flow over a backward-facing step", *J. Fluid Mech.*, Vol. 330, pp. 349-374.

Lowery, P. S., and Reynolds, W. C., 1986, "Numerical simulation of a spatially-developing, forced, plane mixing layer", *Rep. TF-26, Thermosciences Division, Dept. of Mech. Engng*, Stanford University.

Manhart, M., 2004, "A zonal algorithm for DNS of turbulent boundary layers", *Computers and Fluids*, Vol. 33, pp. 435-461.

Moffatt, M. K., 1964, "Viscous and resistive eddies near a sharp corner", *J. Fluid Mech.*, Vol. 18, pp. 1-18.

Morinishi, Y., 2007, "Backward-facing step flow between step-side stationary and moving walls", *Proc. 5th International Symposium on Turbulence and Shear Flow Phenomena, Munich, Germany*, pp. 673-676.

Neto, S. A., Grand, D., Métais, O., and Lesieur, M., 1993, "A numerical investigation of the coherent vortices in turbulence behind a backward-facing step", *J. Fluid Mech.*, Vol. 256, pp. 1-25.

Nychas, G. S., Hershey C. H., and Brodkey, S. R., 1973, "A visual study of turbulent shear flow", *J. Fluid Mech.*, Vol. 61, pp. 513-540.

Rogers, M. M., and Moser, R. D., 1993, "Direct simulation of a self similar turbulent mixing layer", *Phys. Fluids*, Vol. 6, pp. 903-923.